

## Coseismic slip distribution of the February 27, 2010 Mw 8.8 Maule, Chile earthquake

Fred F. Pollitz,<sup>1</sup> Ben Brooks,<sup>2</sup> Xiaopeng Tong,<sup>3</sup> Michael G. Bevis,<sup>4</sup> James H. Foster,<sup>2</sup> Roland Bürgmann,<sup>5</sup> Robert Smalley, Jr.,<sup>6</sup> Christophe Vigny,<sup>7</sup> Anne Socquet,<sup>8</sup> Jean-Claude Ruegg,<sup>8</sup> Jaime Campos,<sup>9</sup> Sergio Barrientos,<sup>9</sup> Héctor Parra,<sup>10</sup> Juan Carlos Baez Soto,<sup>11</sup> Sergio Cimbaro,<sup>12</sup> and Mauro Blanco<sup>13</sup>

Received 15 February 2011; revised 20 March 2011; accepted 28 March 2011; published 6 May 2011.

[1] Static offsets produced by the February 27, 2010  $M_w = 8.8$  Maule, Chile earthquake as measured by GPS and InSAR constrain coseismic slip along a section of the Andean megathrust of dimensions 650 km (in length)  $\times$  180 km (in width). GPS data have been collected from both campaign and continuous sites sampling both the near-field and far field. ALOS/PALSAR data from several ascending and descending tracks constrain the near-field crustal deformation. Inversions of the geodetic data for distributed slip on the megathrust reveal a pronounced slip maximum of order 15 m at  $\sim 15$ – $25$  km depth on the megathrust offshore Lloca, indicating that seismic slip was greatest north of the epicenter of the bilaterally propagating rupture. A secondary slip maximum appears at depth  $\sim 25$  km on the megathrust just west of Concepción. Coseismic slip is negligible below 35 km depth. Estimates of the seismic moment based on different datasets and modeling approaches vary from 1.8 to  $2.6 \times 10^{22}$  N m. Our study is the first to model the static displacement field using a layered spherical Earth model, allowing us to incorporate both near-field and far-field static displacements in a consistent manner. The obtained seismic moment of  $1.97 \times 10^{22}$  N m, corresponding to a moment magnitude of 8.8, is similar to that obtained by previous seismic and

geodetic inversions. **Citation:** Pollitz, F. F., et al. (2011), Coseismic slip distribution of the February 27, 2010 Mw 8.8 Maule, Chile earthquake, *Geophys. Res. Lett.*, 38, L09309, doi:10.1029/2011GL047065.

### 1. Introduction

[2] The February 27, 2010 Maule, Chile earthquake ruptured about 650 km of the Andean megathrust in a bilateral rupture with an epicenter about 60 km south of Constitución (Figure 1). The relative motion between the Nazca and South American plates in this area is 63–68 mm/yr [Kendrick *et al.*, 2003; Vigny *et al.*, 2009; Ruegg *et al.*, 2009]. The interseismic geodetic velocity field measured prior to the earthquake is consistent with nearly 100% of the relative plate motion accumulating as elastic strain which would eventually be released seismically [Ruegg *et al.*, 2009]. Outstanding questions regarding the 2010 earthquake concern: (1) the overall seismic moment; (2) the amount of slip released compared with that thought to have accumulated since the last large subduction event in 1835; and (3) the post-earthquake relaxation to be anticipated following the 2010 event. In this study, we estimate the slip distribution using a combination of Interferometric Synthetic Aperture Radar (InSAR) data and Global Positioning System (GPS) data. These data span distances from a few km to several thousand km from the rupture. We use a layered spherical elastic structure to model the static displacement field, permitting us to use the near-field and far field data in a consistent manner to constrain the coseismic slip distribution.

### 2. Data Set

[3] The observed GPS coseismic displacement field is shown in Figure 2. It is a subset of 396 GPS displacement vectors obtained by processing of pre-event and post-event observations in the ITRF2005 reference frame [Altamimi *et al.*, 2007]. This includes data from the International GPS Service (IGS) and CAP (Central Andes Project) [Brooks *et al.*, 2003; Kendrick *et al.*, 2003; Smalley *et al.*, 2003]. We processed all available continuous GPS data in South America from 2007 through May 5, 2010 using GAMIT [King and Bock, 2005] with additional IGS sites included to provide regional reference frame stability. We defined a South American fixed reference frame, primarily from the Brazilian craton, to better than 2.4 mm/yr rms horizontal velocity by performing daily Helmert transformations for the network solutions and stacking in an ITRF2005 reference frame. With the resultant time series components we used

<sup>1</sup>U.S. Geological Survey, Menlo Park, California, USA.

<sup>2</sup>School of Ocean and Earth Science and Technology, University of Hawaii at Manoa, Honolulu, Hawaii, USA.

<sup>3</sup>Scripps Institution of Oceanography, University of California, San Diego, La Jolla, California, USA.

<sup>4</sup>School of Earth Sciences, Ohio State University, Columbus, Ohio, USA.

<sup>5</sup>Department of Earth and Planetary Sciences, University of California, Berkeley, California, USA.

<sup>6</sup>Center for Earthquake Research and Information, The University of Memphis, Memphis, Tennessee, USA.

<sup>7</sup>Laboratoire de Géologie de l'Ecole Normale Supérieure, UMR 8538, CNRS, Paris, France.

<sup>8</sup>Institut de Physique du Globe de Paris, UMR 7154, Université Paris-Diderot, CNRS, Paris, France.

<sup>9</sup>Departamento de Geofísica, Universidad de Chile, Santiago, Chile.

<sup>10</sup>Departamento de Geodesia, Instituto Geográfico Militar Chile, Santiago, Chile.

<sup>11</sup>Departamento de Ciencias Geodésicas y Geomática, Universidad de Concepción, Concepción, Chile.

<sup>12</sup>Dirección de Geodesia, Instituto Geográfico Nacional Argentina, Buenos Aires, Argentina.

<sup>13</sup>Instituto CEDIAC, Universidad Nacional de Cuyo, Mendoza, Argentina.

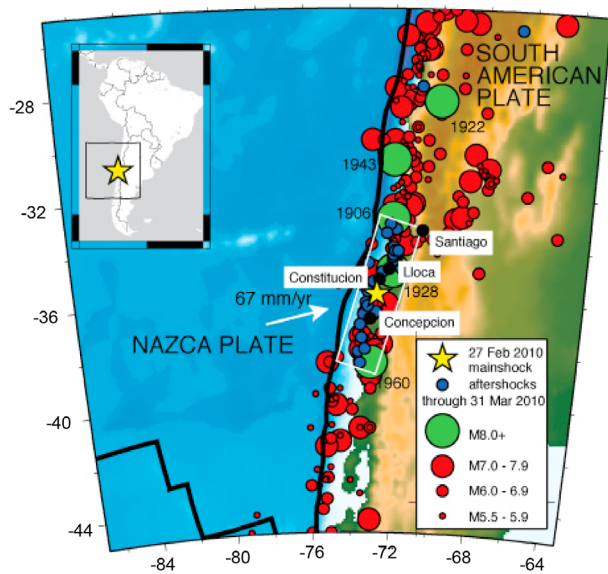


**Figure 1.** Observed coseismic GPS offsets (black vectors) with 95% uncertainties compared with model horizontal offsets using the coseismic slip model obtained by the joint InSAR/GPS inversion, which is contoured in gray (values in meters). White lines indicate the surface projection of the fault plane.

a robust linear regression to fit a two-velocity (pre- and post-earthquake) and step (co-seismic displacements) model (Figure S1 of the auxiliary material).<sup>1</sup> Errors were calculated using residual scatter values. Seventeen additional displacement vectors have been obtained through analysis of continuous sites installed under the framework of the Chilean-French cooperation, the international laboratory ‘Montessus de Ballore.’

[4] The InSAR data consists of ascending and descending Advanced Land Observatory Satellite (ALOS) Phased Array type L-band Synthetic Aperture Radar (PALSAR) data provided by the Japan Aerospace Exploration Agency (JAXA). This consists of ascending interferograms (swath mode) along tracks T111, T113, T114, T117, T118, T119 and descending interferograms (a combination of ScanSAR to swath mode, ScanSAR to ScanSAR and swath mode interferograms) along tracks T422 and T420. Ascending data have satellite-ground vectors oriented approximately  $37^\circ$  from vertical and  $16^\circ$  counterclockwise from due East; descending data have satellite-ground vectors oriented approximately  $37^\circ$  from vertical and  $164^\circ$  counterclockwise from due East. The ALOS interferograms have been processed with the newly developed GMTSAR software at Scripps Institution of Oceanography to produce unwrapped, sampled, and GPS-calibrated line-of-sight displacement (LOS) (Figure S2). Additional details are provided in the auxiliary material of *Tong et al.* [2010].

### 3. The 27 February 2010 Coseismic Slip Model

[5] The fault geometry is that of a single planar surface striking  $N17.5^\circ E$  and dipping  $\delta$  toward the east, where  $\delta$  takes

trial values between  $14$  and  $20^\circ$ . This geometry is based on the Global CMT solution and is similar to that adopted in recent seismic slip inversions. We fix the width of the fault projected to the surface to be  $185$  km. To allow for the possibility of slip extending to the transition zone, we put the lower edge of this plane at  $185 \text{ km} \times \tan \delta$ ; this depth is  $60.1$  km for  $\delta = 18^\circ$ . Distributed slip is represented with a distribution of continuous functions as employed by *Pollitz et al.* [1998]. These are Hermite-Gauss (HG) functions of position on the rectangular fault plane.

[6] Slip on the slab interface is related to static surface displacement using the source response functions calculated with the method of *Pollitz* [1996]. This yields theoretical displacements in a layered spherical geometry with a spherical harmonic expansion, and global Earth model PREM with isotropic elastic parameters, appended by the crustal structure of *Bohm et al.* [2002], is used for this purpose.

[7] Green’s functions for three-dimensional static displacement are evaluated for each HG component of slip on the fault plane (Figure 2) comprising a portion of the megathrust of length  $650$  km, width  $W$ , dip  $\delta$ , strike  $N17.5^\circ E$ , and rake  $112^\circ$ . The strike and rake correspond to the geometry of the Global CMT solution. We consider variable width and dip that covary such that  $W \cos \delta = 185$  km.

[8] GPS and InSAR data are inverted for distributed slip using weighted least squares. In the inversions each GPS datum is assigned its formal uncertainty, while each of the InSAR LOS measurement is assumed independent and identically distributed with a standard error of  $150$  mm. This serves to give the GPS and InSAR data roughly equal weight in the inversions. A small amount of damping of the squared gradient of the slip is used to regularize the inversion and determine the weighting coefficients of the HG functions [*Pollitz et al.*, 1998]. Separate inversions are performed for a dataset consisting of (a) InSAR only, (b) GPS only, and (c) combined InSAR and GPS data. In the inversions with the combined datasets, the best overall fit is obtained with a dip value  $\delta = 18^\circ$  (Figure S3). The resulting slip distributions are shown in Figure 3. Figures 2 and S2 show the corresponding fits to the GPS and InSAR data, respectively, resulting from the joint InSAR/GPS inversion. The seismic moment is  $M_0 = 1.97 \times 10^{22}$  N m, corresponding to a moment magnitude of  $8.83$ .

### 4. Discussion

[9] Horizontal GPS coseismic offsets are fit well at both near-field distance and far-field distance (the boxed regions in Figure 2), a result that is attributable to the use of a spherically-layered elastic structure in our model. Average residuals (including both North and East components) are  $1.5$  cm and  $0.3$  cm for the near-field and far-field GPS data, respectively. Average residuals for the ascending and descending InSAR LOS data are  $9.9$  cm and  $8.3$  cm, respectively.

[10] In all cases, the slip distribution exhibits a pronounced maximum  $\sim 19$  m at  $\sim 15$ – $25$  km depth on the megathrust offshore Lloca (Figure 1), and slip is generally confined to the upper  $35$  km of the interplate boundary. A secondary maximum of  $\sim 9$  meters is located about  $250$  km further south at depth  $\sim 25$  km on the megathrust west of Concepción. The GPS and InSAR datasets are highly complementary, the InSAR data providing better near-field coverage and the GPS data better far-field coverage. Nevertheless, the resulting slip

<sup>1</sup>Auxiliary materials are available in the HTML. doi:10.1029/2011GL047065.

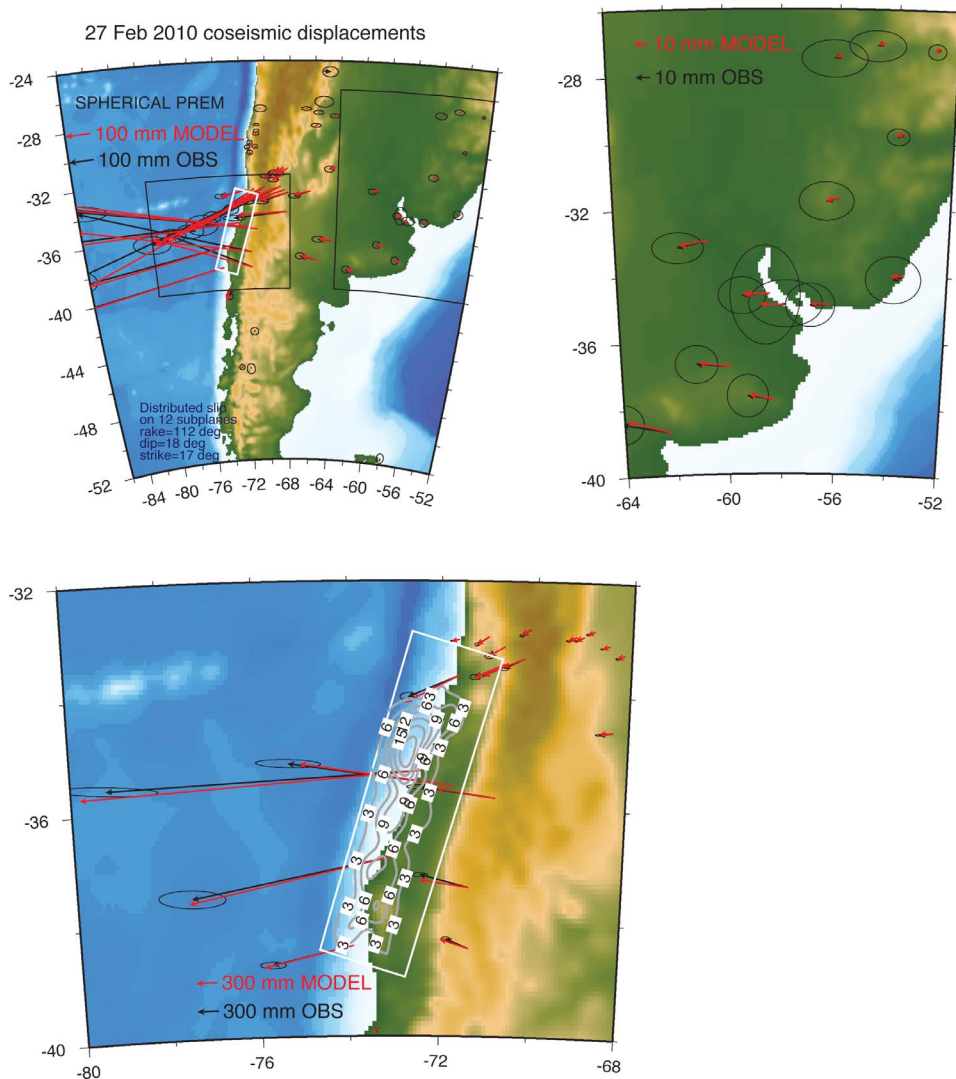


**Figure 2.** Coseismic slip models derived from (a) InSAR data only, (b) GPS data only, and (c) combined GPS and InSAR data, with seismic moment indicated for each model. Contour interval is 3 m. Star symbol indicates the Global CMT epicenter.

distribution is determined primarily by InSAR. Inversion using only GPS (Figure 3b) does not localize the slip as effectively as the inversion with InSAR alone or both data types (Figures 3a and 3c). Resolution of inverted slip is addressed by constructing synthetic data sets using input slip distributions (Figures S4a and S4c) and inverting them in the same manner as the actual data. The inverted slip distributions in Figures S4b and S4d show that average slip over all but the shallowest  $\sim 15$  km of the rupture plane may be adequately estimated. It also shows that any significant slip below  $\sim 35$  km depth, if it existed, would be imaged using the present dataset.

[11] Table S1 summarizes the results of several recent studies. *Lay et al.* [2010] derived slip distributions of the earthquake based on long-period seismic waveform data (P, SH, and short-arc Rayleigh waves) at periods up to  $\sim 200$  s. *Delouis et al.* [2010] derived a slip distribution using a combination of GPS, InSAR, seismic waveform data (P and SH waves) at periods  $\sim 30$  to 200 sec, including high-rate GPS data at regional distance. *Tong et al.* [2010] derived a slip

distribution using a GPS and InSAR data set similar to that presented here. Our slip distribution and those of *Lay et al.* [2010], *Delouis et al.* [2010], *Tong et al.* [2010], and *Lorito et al.* [2011] are similar in terms of the spatial pattern, including the location of both the primary slip maximum near  $35^{\circ}\text{S}$ ,  $72.6^{\circ}\text{W}$  at about 20 km depth and a secondary slip maximum near  $37^{\circ}\text{S}$ ,  $73.5^{\circ}\text{W}$ . Our obtained  $M_0$  is near the lower end of the range  $2.1\text{--}2.6 \times 10^{22}$  N m in *Lay et al.*'s [2010] models, which use combinations of P and SH body-wave information. Trial inversions by G. Shao (Preliminary slip model of the Feb 27, 2010 Mw 8.9 Maule, Chile, earthquake, 2010, available at [http://www.geol.ucsb.edu/faculty/ji/big\\_earthquakes/2010/02/27/chile\\_227.html](http://www.geol.ucsb.edu/faculty/ji/big_earthquakes/2010/02/27/chile_227.html)) and *Lay et al.* [2010] indicate that the seismic inversions are sensitive to the types of waveform data being included and the frequency band.

[12] The  $M_0$  inferred here ( $1.97 \times 10^{22}$  N m) based on the static displacement field exceeds the GCMT estimate ( $1.8 \times 10^{22}$  N m) [*Ekström et al.*, 2005; *Dziewonski et al.*, 1981] by about 10%, possibly because of early afterslip, which may

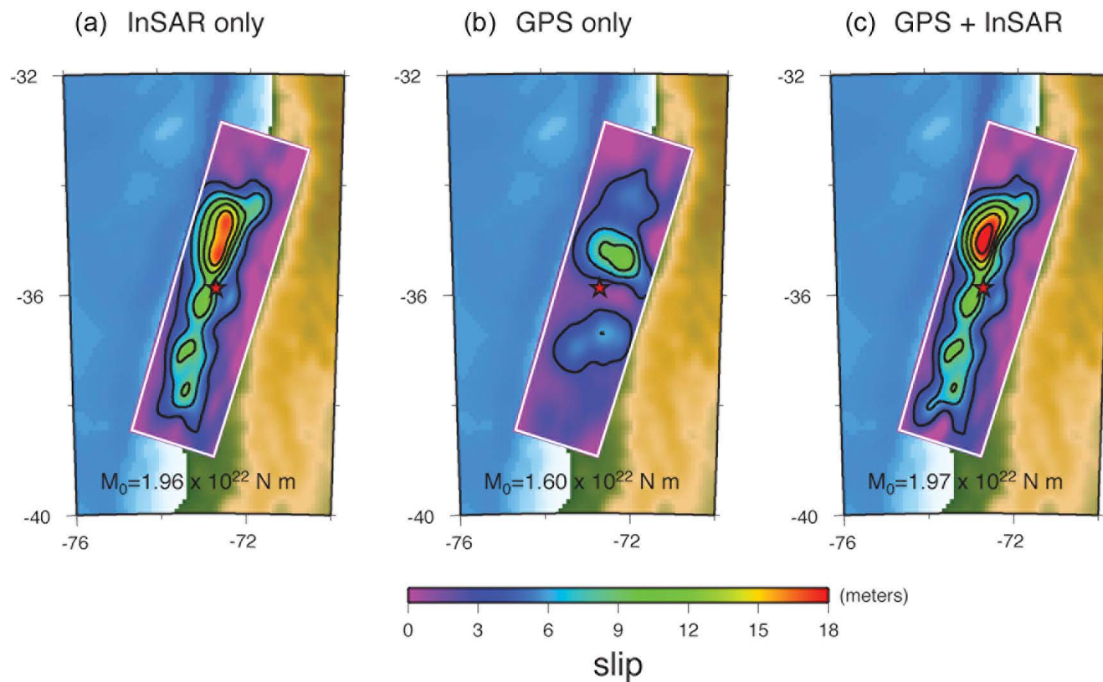


**Figure 3.** Rupture areas associated with historic earthquakes along the Andean megathrust and aftershocks of the February 27, 2010 event. Historical epicenters are provided by Centro Regional de Sismología para America del Sur and aftershock locations are provided by the National Earthquake Information Center. White lines indicate the surface projection of the fault plane used to model the 2010 event. Nazca - South America relative plate motion vector is from *Ruegg et al.* [2009].

have contributed up to an additional 26% to the seismic moment based on shorter period (<350 sec) seismic waves alone [Tanimoto and Ji, 2010]. *Okal et al.* [2010], however, conclude that the normal mode data is consistent with the GCMT moment. Although the seismic moment remains to be reconciled between seismic and geodetic studies, both the seismic and geodetic data can be explained to a large extent using a slip-time function that is not unusually long, e.g., 120–150 s in Figure 4 of *Lay et al.* [2010] or Figure 3 of *Delouis et al.* [2010].

[13] The  $1.8 \times 10^{22}$  N m value obtained by both *Delouis et al.* [2010] and *Tong et al.* [2010] is about 10% lower than our estimated  $M_0$ . Although those studies use a homogeneous half-space in modeling the geodetic data, inversion of the present dataset using a homogeneous sphere with shear modulus of 40 GPa (that used by *Tong et al.* [2010]) slightly increases  $M_0$  from  $1.97$  to  $2.05 \times 10^{22}$  N m. Estimated  $M_0$  based on the static displacement field is also sensitive to fault dip (Figure S3). Inversion of the present dataset using a dip of  $15^\circ$  (that used by *Tong et al.* [2010]) results in  $M_0 = 1.79 \times 10^{22}$  N m, in agreement with the above geodetic studies. Nevertheless, the inclusion of sphericity and layering is important. For example, the use of a homogeneous sphere in our modeling results in a slip distribution that is biased toward shallower depths (compare Figure 3 with Figure S5) and cannot simultaneously fit both near-field and far-field GPS data (Figure S6).

[14] The area that ruptured in the earthquake coincides with a highly locked zone as inferred from pre-earthquake geodetic measurements [Brooks et al., 2003; Ruegg et al., 2009; Moreno et al., 2010]. The maximum and average slip on

the megathrust shallower than 35 km are 18.8 and 6.8 m, respectively. These values may be compared with the amount of slip that has accumulated since the last major earthquake in 1835, which amounts to about 11–12 m assuming 100% interplate coupling and a 63–68 mm/yr relative plate motion. The exceedance of maximum slip (in the shallow portion of the megathrust north of the epicenter) over post-1835 accumulated slip may reflect relatively low slip in the 1835 event, so that the present slip distribution includes some slip accumulated prior to 1835. On the other hand, the preponderance of slip <8 m over most of the megathrust in the 2010 event, particularly in the ‘Darwin gap’ between  $\sim 36^\circ$  and  $37.5^\circ$ S, requires another mechanism for releasing the expected slip, such as slow slip event(s) between 1835 and 2010, or it may indicate a remaining slip deficit [Lorito et al., 2011].

[15] **Acknowledgments.** We thank the Instituto Brasileiro de Geografia e Estatística (IBGE) for access to RBMC Brazil continuous GPS network data. We are grateful to Thorne Lay and an anonymous reviewer and Eric Calais for their constructive criticisms.

[16] The Editor thanks Thorne Lay and an anonymous reviewer for their assistance in evaluating this paper.

## References

- Altamimi, Z., X. Collilieux, J. Legrand, B. Garayt, and C. Boucher (2007), ITRF2005: A new release of the International Terrestrial Reference Frame based on time series of station positions and Earth Orientation Parameters, *J. Geophys. Res.*, *112*, B09401, doi:10.1029/2007JB004949.
- Bohm, M., S. Lüth, H. Echtler, G. Asch, K. Bataille, C. Bruhn, A. Rietbrock, and P. Wigger (2002), The Southern Andes between  $36^\circ$  and  $40^\circ$  latitude: Seismicity and average seismic velocities, *Tectonophysics*, *356*, 275–289.

- Brooks, B. A., M. Bevis, R. Smalley Jr., E. Kendrick, R. Manceda, E. Lauría, R. Maturana, and M. Araujo (2003), Crustal motion in the Southern Andes (26°–36°S): Do the Andes behave like a microplate?, *Geochem. Geophys. Geosyst.*, 4(10), 1085, doi:10.1029/2003GC000505.
- Delouis, B., J.-M. Nocquet, and M. Vallée (2010), Slip distribution of the February 27, 2010 Mw = 8.8 Maule earthquake, central Chile, from static and high-rate GPS, InSAR, and broadband teleseismic data, *Geophys. Res. Lett.*, 37, L17305, doi:10.1029/2010GL043899.
- Dziewonski, A. M., T.-A. Chou, and J. H. Woodhouse (1981), Determination of earthquake source parameters from waveform data for studies of global and regional seismicity, *J. Geophys. Res.*, 86, 2825–2852.
- Ekström, G., A. M. Dziewonski, N. N. Maternovskaya, and M. Nettles (2005), Global seismicity of 2003: centroid-moment-tensor solutions for 1087 earthquakes, *Phys. Earth Planet. Inter.*, 148, 327–351.
- Kendrick, E., M. Bevis, R. J. Smalley, B. Brooks, R. B. Vargas, E. Laura, and L. P. S. Fortes (2003), The Nazca-South America Euler vector and its rate of change, *J. South Am. Earth Sci.*, 16, 125–131.
- King, R., and Y. Bock (2005), Documentation for the GAMIT GPS analysis software, release 10.2, Mass. Inst. of Technol., Cambridge.
- Lay, T., C. J. Ammon, H. Kanamori, K. D. Koper, O. Sufri, and A. R. Hutko (2010), Teleseismic inversion for rupture process of the 27 February 2010 Chile (M<sub>w</sub> 8.8) earthquake, *Geophys. Res. Lett.*, 37, L13301, doi:10.1029/2010GL043379.
- Lorito, S., F. Romano, S. Atzori, X. Tong, A. Avallone, J. McCloskey, M. Cocco, E. Boschi, and A. Piatanesi (2011), Limited overlap between the seismic gap and coseismic slip of the great 2010 Chile earthquake, *Nat. Geosci.*, 4, 173–177.
- Moreno, M., M. Rosenau, and O. Oncken (2010), 2010 Maule earthquake slip correlates with pre-seismic locking of Andean subduction zone, *Nature*, 467, 198–204.
- Okal, E., S. Hongsresawat, and S. A. Stein (2010), Normal modes excited by the 2010 Chile earthquake: no evidence for an ultra-slow component to the source, Abstract U21B–06 presented at 2010 Fall Meeting, AGU, San Francisco, Calif., 13–17 Dec.
- Pollitz, F. (1996), Coseismic deformation from earthquake faulting on a layered spherical earth, *Geophys. J. Int.*, 125, 1–14.
- Pollitz, F. F., R. Bürgmann, and P. Segall (1998), Joint estimation of after-slip rate and postseismic relaxation following the 1989 Loma Prieta earthquake, *J. Geophys. Res.*, 103, 26,975–26,992.
- Ruegg, J. C., A. Rudloff, C. Vigny, R. Madariaga, J. B. de Chabaliere, C. Campos, E. Kausel, S. Barrientos, and D. Dimitrov (2009), Inter-seismic strain accumulation measured by GPS in the seismic gap between Constitución and Concepción, *Phys. Earth Planet. Inter.*, 175, 78–85.
- Smalley, R., Jr., E. Kendrick, M. G. Bevis, I. W. D. Dalziel, F. Taylor, E. Lauría, R. Barriga, G. Casassa, E. Olivero, and E. Piana (2003), Geodetic determination of relative plate motion and crustal deformation across the Scotia-South America plate boundary in eastern Tierra del Fuego, *Geochem. Geophys. Geosyst.*, 4(9), 1070, doi:10.1029/2002GC000446.
- Tanimoto, T., and C. Ji (2010), Afterslip of the 2010 Chilean earthquake, *Geophys. Res. Lett.*, 37, L22312, doi:10.1029/2010GL045244.
- Tong, X., et al. (2010), The 2010 Maule, Chile earthquake: Down-dip rupture limit revealed by space geodesy, *Geophys. Res. Lett.*, 37, L24311, doi:10.1029/2010GL045805.
- Vigny, C., A. Rudloff, J.-C. Ruegg, R. Madariaga, J. Campos, and M. Alvarez (2009), Upper plate deformation measured by GPS in the Coquimbo Gap, Chile, *Phys. Earth Planet. Inter.*, 175, 86–95.
- S. Barrientos and J. Campos, Departamento de Geofísica, Universidad de Chile, Blanco Encalada 2086, Santiago, CP 8370449, Chile.
- M. G. Bevis, School of Earth Sciences, Ohio State University, 125 South Oval Mall, Columbus, OH 43210, USA.
- M. Blanco, Instituto CEDIAC, Universidad Nacional de Cuyo, Parque General San Martín CC 405 (5500) Mendoza, Argentina.
- B. Brooks and J. H. Foster, School of Ocean and Earth Science and Technology, University of Hawaii at Manoa, 1680 East West Rd., Honolulu, HI 96822, USA.
- R. Bürgmann, Department of Earth and Planetary Sciences, University of California, 307 McCone Hall #4767, Berkeley, CA 94720-4767, USA.
- S. Cimbaro, Dirección de Geodesia, Instituto Geográfico Nacional Argentina, Avda. Cabildo 381 (1426), Buenos Aires, Argentina.
- H. Parra, Departamento de Geodesia, Instituto Geográfico Militar Chile, Nueva Santa Isabel 1640, Santiago, Chile.
- F. F. Pollitz, U.S. Geological Survey, 345 Middlefield Rd., MS 977, Menlo Park, CA 94025, USA. (fpollitz@usgs.gov)
- J.-C. Ruegg and A. Socquet, Institut de Physique du Globe de Paris, UMR 7154, Université Paris-Diderot, CNRS, 4 place Jussieu, F-75252 Paris CEDEX, France.
- R. Smalley, Jr., Center for Earthquake Research and Information, The University of Memphis, 3876 Central Ave., Ste. 1, Memphis, TN 38152-3050, USA.
- J. C. B. Soto, Departamento de Ciencias Geodésicas y Geomática, Universidad de Concepción, Juan Antonio Coloma 0201, Concepción, Chile.
- R. Tong, Scripps Institution of Oceanography, University of California, San Diego, 1101 Biological Grade, La Jolla, CA 92037, USA.
- C. Vigny, Laboratoire de Géologie de l'École Normale Supérieure, UMR 8538, CNRS, 24 rue Lhomond, F-75231 Paris CEDEX 05, France.